Journal of Magnetic Resonance **153,** 238–245 (2001)
doi:10.1006/jmre.2001.2439, available online at http://www.idealibrary.com on IDEAL®

Single-Crystal ^{57}Fe Q-Band ENDOR Study of the 4 Iron–4 Sulfur Cluster in its Reduced [4Fe–4S]$^{1+}$ State

Fabrice Moriaud,[1] Serge Gambarelli, Bernard Lamotte, and Jean-Marie Mouesca

Service de Chimie Inorganique et Biologique, UMR 5046, Département de Recherche Fondamentale sur la Matière Condensée, CEA-Grenoble, 17 rue des Martyrs, 38054 Grenoble Cedex 9, France

E-mail: mouesca@drfmc.ceng.cea.fr

Received May 1, 2001; revised August 30, 2001

^{57}Fe Q-band ENDOR has been used to study the [4Fe–4S]$^{1+}$ state created by γ irradiation of single crystals of the synthetic model compound $[N(C_2H_5)_4]_2[Fe_4S_4(SCH_2C_6H_5)_4]$ enriched in ^{57}Fe. This compound is an excellent biomimetic model of the active sites of many 4 iron–4 sulfur proteins, enabling detailed and systematic studies of its oxidized [4Fe–4S]$^{3+}$ and reduced [4Fe–4S]$^{1+}$ paramagnetic states. Taking advantage of the fact that Q-band ENDOR, in contrast with X-Band ENDOR, allows for a very good separation of the ^{57}Fe transitions from those of the protons, the complete hyperfine tensors of the four iron atoms for the [4Fe–4S]$^{1+}$ species has been measured with precision. For each iron atom, the electron orbital and electron spin isotropic contributions have been determined separately. Moreover, it is remarkable that two ^{57}Fe hyperfine tensors attributed to the ferrous pair of iron atoms are very different. In effect, one tensor presents a much larger anisotropic part and a much smaller isotropic part than those of the other. This difference has been interpreted in terms of a differential electron orbital hyperfine interaction among the two ferrous ions. © 2001 Elsevier Science

I. INTRODUCTION

The most common and representative prosthetic site of iron–sulfur proteins performing quite diverse electron-transfer and enzymatic functional roles (*1–3*) is the 4Fe–4S cubane-type cluster. Three naturally occuring redox states are known: [4Fe–4S]$^{3+}$, [4Fe–4S]$^{2+}$, and [4Fe–4S]$^{1+}$, the former two being involved in high-potential iron–sulfur proteins (HiPIP) and the latter two in ferredoxin electron transfer proteins (and others). These are all mixed-valence states involving, formally, 1 Fe^{2+} and 3 Fe^{3+}, 2 Fe^{2+} and 2 Fe^{3+}, and 3 Fe^{2+} and 1 Fe^{3+} ions, respectively.

Mössbauer, EPR, ENDOR, and NMR are the main spectroscopic methods used for the characterization and study of these redox states. Moreover, hyperfine interactions are the most important observables accessible to these methods since they give access to the electron spin density mapping on the cluster atoms and on their vicinal amino acid ligands, generally cysteines. As ^{56}Fe and ^{32}S nuclei have zero nuclear spin, only three nuclei remain as affordable and potential probes for measuring their hyperfine interactions with the unpaired electron spin density: ^{57}Fe at the level of the cluster itself and the closest protons and ^{13}C belonging to the CH_2 groups at the level of the ligands.

The information gained from ^{57}Fe Mössbauer or ENDOR spectroscopies in frozen solution is, indeed, of primary importance. However, they suffer from some limitations essentially due to the fact that the experiments are performed on frozen solutions. The resolution is relatively poor and the determination of the tensors is incomplete, as the eigendirections are missing.

This is why, when feasible, single crystals are used. Systematic studies have been developped under the best conditions of resolution for the two paramagnetic states [4Fe–4S]$^{3+}$ and [4Fe–4S]$^{1+}$, relying on an approach based on EPR (*4–6*) and ENDOR (*7–11*) studies of single crystals of good [4Fe–4S] synthetic analogues of the proteins prosthetic sites. These analogues were synthesized in the diamagnetic [4Fe–4S]$^{2+}$state, the paramagnetic species being created (at low concentration) by γ radiation of these single crystals. These species correspond to trapped holes (the [4Fe–4S]$^{3+}$ centers) and trapped electrons (the [4Fe–4S]$^{1+}$ centers) simultaneously formed in the crystal (*4–6*). Compound (I), $[N(C_2H_5)_4]_2[Fe_4S_4(SCH_2C_6H_5)_4]$, is the most convenient model compound for these studies, since its thiolate CH_2 groups simulate quite well those of cysteins in the proteins. The EPR signals of the [4Fe–4S]$^{3+}$ centers in the crystals of this compound are, after irradiation, more intense (by a factor of 5 to 10) than those of the [4Fe–4S]$^{1+}$ centers and have been studied already by ^{57}Fe ENDOR (*7*) and later by proton ENDOR (*8, 12*).

However, it was imperative to develop the same studies on the [4Fe–4S]$^{1+}$ state and, if possible, on the same compound. In effect, this paramagnetic 1+ state plays a major role in most of the iron–sulfur proteins. It is also the most challenging in terms of its magnetic properties. We wish to present in this article the study, by ^{57}Fe Q-band ENDOR, of a [4Fe–4S]$^{1+}$reduced state

[1] Now at the Biophysics Department of Leiden University, Huygens Laboratory, P.O. Box 9504, 2300 RA Leiden, The Netherlands.

1090-7807/01 $35.00

obtained from γ irradiating a single crystal of the previously mentioned compound (I). The reduced center studied in this paper had previously been called (*5*) I_R. This study is closely related to that of the same species in the same compound that we recently completed by proton ENDOR at Q-Band (*11*).

II. EXPERIMENTAL SECTION

(1) Preparation of $[N(C_2H_5)_4]_2[^{57}Fe_4S_4(SCH_2C_6H_5)_4]$ Single Crystals

Compound (I), enriched at 95% in ^{57}Fe was prepared as described previously (*7*). Single crystals, weighing between 2 and 3 mg, were used. These were obtained, as before (*7, 8*), by a transport method in a solution of the compound in acetonitrile. They were then irradiated up to doses of about 1 MGy by γ rays in a ^{60}Co source at room temperature, under argon atmosphere. The crystallographic structure of this compound at room temperature has been published by Averill *et al.* (*13*). It corresponds to the monoclinic space group $P2\,1/c$ with $Z = 4$. The structure of the cubane cluster and of the terminal parts of its thiolate ligands is presented in Fig. 1, the atoms being labeled according to the Averill structure determination. Single crystals generally grow with a well-developed face corresponding to the *ac* plane, its greatest dimension being along the *a* axis. An orthogonal reference frame with axes a, b, and c^* is defined from this morphology, the last axis being defined as perpendicular to the two others. These elements are used to orient our single crystals and to study their EPR and ENDOR spectra in the three mutually orthogonal planes ab, bc^*, and ac^*. Each paramagnetic center exhibits two inequivalent sites for a general orientation of the static magnetic field with respect to the orientations of the unit cell. These two sites become equivalent in the EPR and ENDOR spectra when the magnetic field vector either is contained in the mirror glide plane *ac* or is aligned along the *b* screw axis.

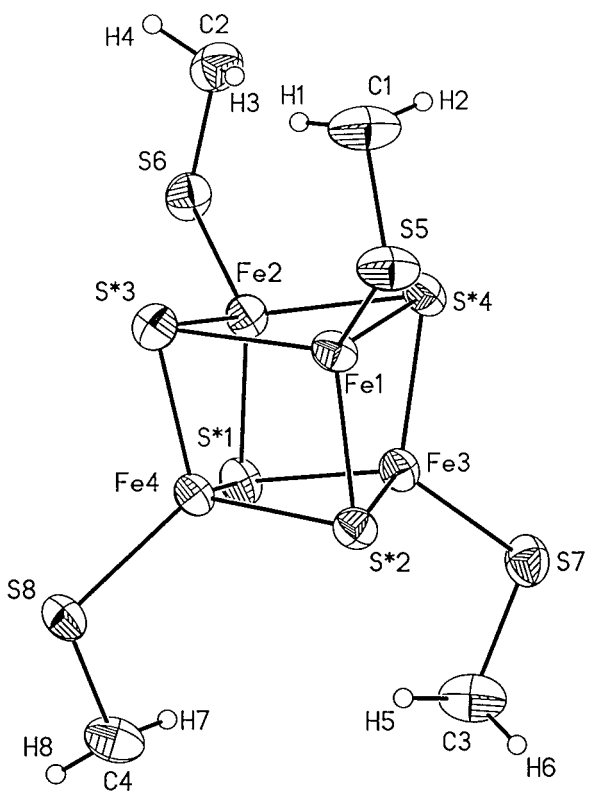

FIG. 1. Structure of the $Fe_4S_4(SCH_2C_6H_5)_4$ core.

(2) ENDOR Methodology

Q-band ENDOR experiments were performed on a Bruker ESP 300 spectrometer with an CF 935 flow helium cryostat used to maintain the samples at the temperature giving the most intense ENDOR lines (i.e., 8 K). An old model of the ER 5106 QT variable temperature EPR Bruker cavity, leaving access to sample holders up to 3 mm in diameter, was adapted for ENDOR. We used a sample holder made from a 3-mm diameter Perspex cylinder with a tooled flat vertical surface for the sample, on which the single turn ENDOR loop (a 0.3-mm copper wire) is fixed and glued in a thin groove inscribed on its sides, as previously carried out by G. Denninger (*14*). It is connected via coaxial cables to a 100-W ENI 3100 L broadband RF power amplifier. The single crystal is glued by Apiezon N grease and oriented manually on the tooled plane of the holder. This probe is then introduced with precision to the entrance of the cavity such that its Q-factor does not become less than 2500. The fact that the sample and the copper loop are both fastened to the Perspex rod presents the inconvenience that they rotate together during the studies of the angular dependences of the ENDOR lines. In principle, the radiofrequency field generated by the ENDOR coil must be perpendicular to the static magnetic field. However, we have verified that, most often, sufficient ENDOR signals were obtained for the largest part of the orientations, the component of the radiofrequency field along the perpendicular direction being sufficient for that purpose.

III. EXPERIMENTAL RESULTS

The paramagnetic reduced center I_R studied here is characterized by a **g** tensor with the principal values $g_1 = 2.043$, $g_2 = 1.948$, and $g_3 = 1.871$ (*5*). A Q-band ENDOR spectrum of the eight ^{57}Fe transitions corresponding to its four iron cluster atoms is presented in Fig. 2. The lines are very sharp, indicating that the resolution is therefore very good.

Angular variations of the ENDOR transitions are reported in Figs. 3a–3d. Due to the existence of the two magnetically inequivalent sites, both of the ENDOR transitions obtained separately on the two sites of the EPR lines in each plane are reported. Since the nuclear spin of ^{57}Fe is $\frac{1}{2}$ and its hyperfine interactions a_{Fe} are much larger than its nuclear Zeeman term ν_{Fe} (to first approximation), two ENDOR transitions $\nu_+ \approx a_{Fe}/2 + \nu_{Fe}$ and $\nu_- \approx a_{Fe}/2 - \nu_{Fe}$ are observed for each iron atom, separated by

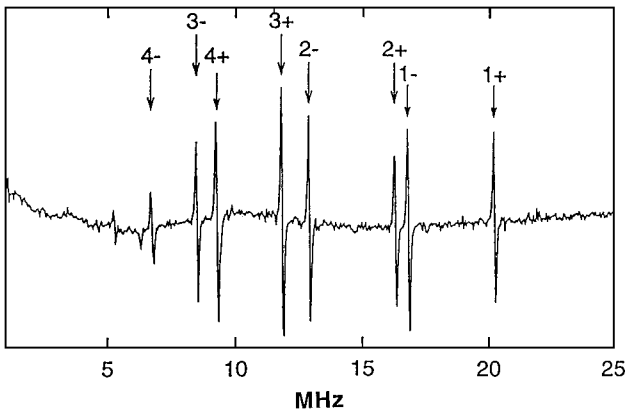

FIG. 2. ^{57}Fe Q-band ENDOR spectrum of the $[4Fe–4S]^{1+}$ center I_R obtained from a γ-irradiated single crystal of the $[N(C_2H_5)_4]_2$ $[Fe_4S_4(SCH_2C_6H_5)_4]$ compound, enriched in ^{57}Fe, when the magnetic field is at 35° from *b* in the *bc** plane.

$2\nu_{Fe} \approx 2.7$ MHz. One must note that ENDOR transitions are missing for some portions of orientations. This happens, either for orientations where the radiofrequency field generated by our ENDOR loop makes a small angle with the static magnetic field or from the fact that the EPR line of this center I_R is, for these orientations, concealed by those of the more intense $[4Fe–4S]^{3+}$ centers (*5*).

While we succeeded in orienting correctly the crystal in the *bc** and *ac** planes, only ENDOR spectra in a so-called *a′b′* plane have been recorded, due to experimental difficulties in the crystal orientation. However, from the EPR line angular variation in the same plane, and from the knowledge of the **g** tensor, it has been possible to correct for this slight disorientation effect (*a′* lies at ≈3° from the "true" *a* axis, and *b′* lies at ≈8° from the "true" *b* axis). All hyperfine tensors in this paper have been corrected and are expressed with respect to the (*a*, *b*, *c**) reference frame.

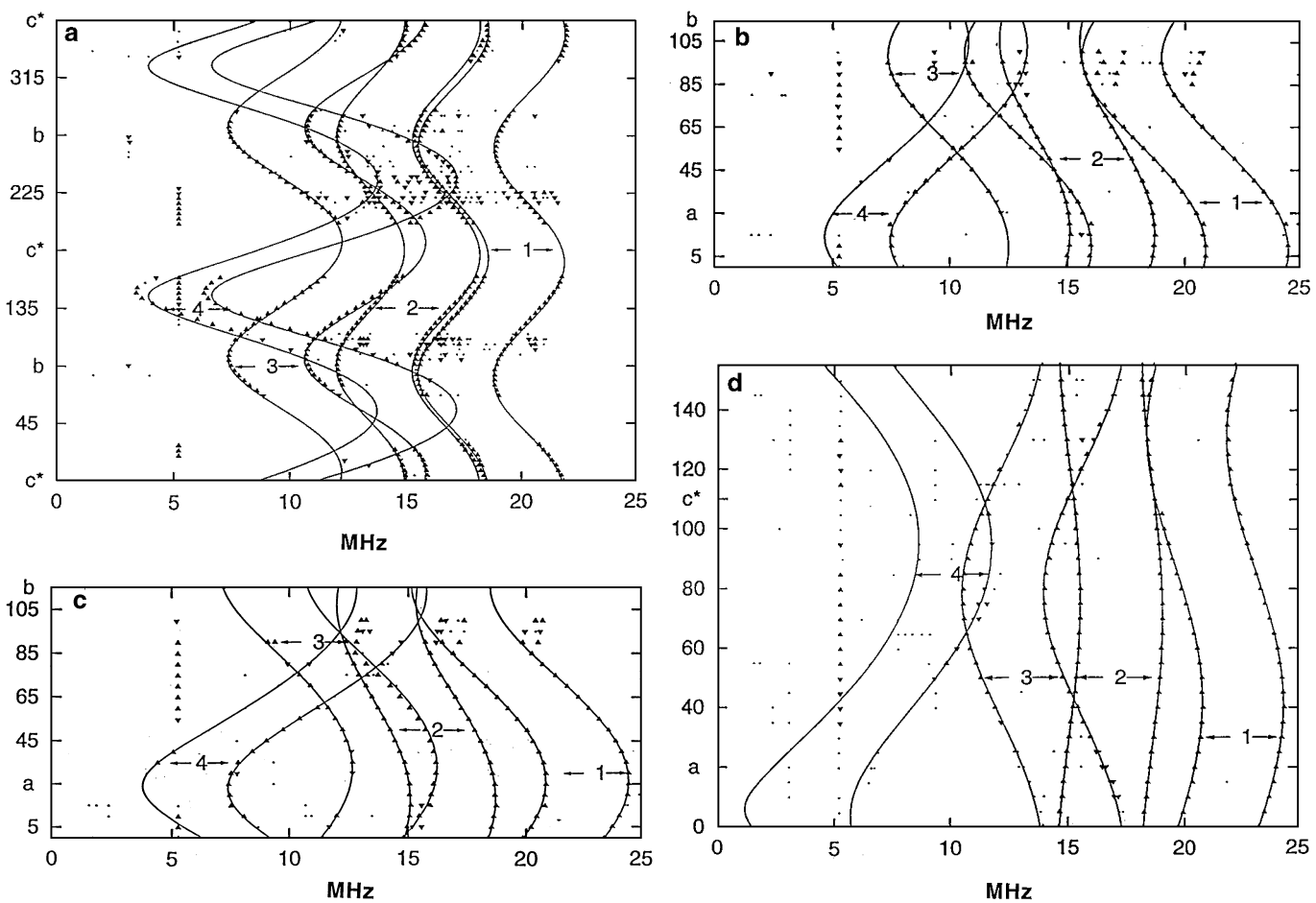

FIG. 3. Experimental points and fits (continuous lines) of the angular dependences of the frequencies of the ^{57}Fe ENDOR transitions at *Q*-band in the three planes *bc** (a), *a′b′* (b) low-field site (c) high-field site, and *c***a* (d). The optimized parameters for the fitting curves are given in the Appendix.

A salient feature appears in Figs. 3a–3d: while the curves corresponding to transitions marked 1 to 3 exhibit anisotropies of relatively similar magnitude, the anisotropy of those corresponding to transitions 4 is much larger. It must be also pointed out that these transitions 4 are much less intense than the others, and are therefore missing for portions of orientations larger than those observed for the three others. This is especially the case for the low-frequency transition 4 that we could not detect at all in the ac^* plane (Fig. 3d) and for which we could only obtain three points in the ab plane (i.e., one for the low-field EPR site and two for the high-field EPR site: cf. Figs. 3b, 3c). In effect, it was critical to obtain these points in order to ascertain the attribution of the high-frequency (ν_+) curve 4 to the fourth ^{57}Fe of the cluster. In fact, we had to recourse to TRIPLE ENDOR, thus irradiating at the frequency of the ν_+ transition of curve 4. We could then observe, about 2.7 MHz lower, the associated ν_- ENDOR line emerging from the noise. Of course, it is notorious that ENDOR intensities are usually difficult to predict. Moreover, they are expected to be smaller at lower frequencies, as is the case for transitions 4 with respect to the others. It is still rather paradoxical that both ν_+ and ν_- transitions 4 could be easily detected down to 3 MHz in the bc plane (cf. Fig. 3a) while none could be seen around 8 to 10 MHz in the ab (Figs. 3b and 3c) and ac^* (Fig. 3d) planes.

In order to deduce the four ^{57}Fe hyperfine tensors from the angular variations of the lines of Figs. 3a–3d, the ^{57}Fe hyperfine tensors **A** were extracted from a precise procedure taking into account the **g** and hyperfine tensors' anisotropies at once, that is, from

$$(\nu_-)^2 - (\nu_+)^2 = (\nu_n/g)(\mathbf{gA} + \mathbf{Ag}), \qquad [1]$$

where ν_n is corrected for the magnetic field variation (*15, 16*). Equation [1] was directly solved for **A** for Tensors 1 to 3. For Tensor 4 however, one could only rely on the high-field transitions in the three planes, and thus derive the six hyperfine parameters from a minimization procedure. More explicit expressions for the high-field frequency, given by Schweiger *et al.* (*15, 16*), were thus used. It can be verified on Figs. 3a –3d that the agreement between fit curves and experimental points is excellent for the tensors 1 to 3. It is slightly less good for tensor 4, as can be seen around the minima of ν_+ and ν_- in the bc^* plane, at $\approx 30^\circ$ from the c^* axis (cf. Fig. 3a).

From these fits and after diagonalization, the four ^{57}Fe hyperfine tensors presented in Table 1 were obtained. These tensors are labeled 1 to 4 in this table in order of decreasing magnitude of their isotropic hyperfine interactions, their attributions to the four iron atoms of the crystallographic structure remaining open. Their relative signs have been determined by TRIPLE ENDOR experiments. These experiments established that the tensors $\mathbf{A}_1$ and $\mathbf{A}_2$ have the same sign, opposite to that of $\mathbf{A}_3$ and $\mathbf{A}_4$.

TABLE 1

Eigenvalues (Complete Tensor, Isotropic, and Anisotropic Parts, in MHz) and Eigenvectors (Direction Cosines along the a^*, b, and c Axes) of the Four Measured ^{57}Fe Hyperfine Tensors

	Principal values (in MHz)			Principal directions: direction cosines with respect to		
Tensors	Total	Isotropic part	Anisotropic part	$\vec{a}$	$\vec{b}$	$\vec{c}^*$
	−46.4		−5.5	+0.984	−0.161	−0.077
A_1	−41.1	−40.9	−0.2	+0.045	−0.195	+0.980
	−34.8		+6.1	+0.173	+0.968	+0.184
	−35.1		−3.0	+0.843	−0.041	−0.537
A_2	−33.1	−32.1	−1.0	+0.537	−0.020	+0.844
	−28.0		+4.1	+0.046	+0.999	−0.005
	+31.3		+6.5	+0.667	−0.035	+0.744
A_3	+25.5	+24.8	+0.7	+0.706	−0.289	−0.647
	+17.7		−7.1	+0.237	+0.957	−0.168
	+31.1		+14.1	−0.0537	+0.817	+0.575
A_4	+14.9	+17.0	−2.1	+0.796	+0.382	−0.469
	+5.1		−11.9	+0.603	−0.433	+0.670

IV. ANALYSIS AND DISCUSSION OF THE RESULTS

(1) Preliminary Remarks

Let us recall first that this reduced state is, to first approximation, built from two distinct pairs of iron atoms, a (usually) delocalized mixed-valence pair $Fe^{2.5+}$–$Fe^{2.5+}$ and a ferrous pair Fe^{2+}–Fe^{2+}. Our previous **g** tensor analysis (*6*) suggested that the mixed-valence pair is located either on the Fe_1–Fe_2 pair on on the Fe_3–Fe_4 pair, following the iron labeling introdiced in the crystallographic structure (*13*) (cf. Fig. 1).

Since absolute signs of hyperfine couplings cannot be determined by ENDOR, one must rely on other sources of information to fix the signs given in Table 1. Firstly, the results of Mössbauer's studies on proteins with their active sites in the $[4Fe–4S]^{1+}$ state (*17, 18*), indicate that two iron atoms, corresponding to the mixed-valence pair, have tensors of negative sign with the largest magnitude, while those pertaining to the ferrous pair are overall positive and of smaller magnitude. Therefore, tensors $\mathbf{A}_1$ and $\mathbf{A}_2$ are attributed to the mixed-valence pair ions while tensors $\mathbf{A}_3$ and $\mathbf{A}_4$ correspond to the ferrous pair ions. The results obtained by proton ENDOR of the same species (*11*) indicate that the mixed-valence pair is located on Fe_1 and Fe_2. This establishes, by combining results of both ^{57}Fe and ^{1}H experiments, that tensors $\mathbf{A}_1$ and $\mathbf{A}_2$ must be attributed to Fe_1 and Fe_2 and tensors $\mathbf{A}_3$ and $\mathbf{A}_4$ to Fe_3 and Fe_4. At this stage, it is not possible to attribute individual hyperfine tensors within each pair to definite iron ions.

Comparison of these ^{57}Fe hyperfine tensors with those obtained for the $[4Fe–4S]^{3+}$ state in the same compound (*7*) shows a relative similarity of the isotropic parts for the two pairs, as well as of their anisotropic parts when considering the mixed-valence pairs. The big difference concerns, as expected, the anisotropic eigenvalues of the ferrous pair of the reduced center I_R, which

are of magnitude much larger than that of the ferric pair in the oxidized $[4Fe–4S]^{3+}$ center (*7*). Another peculiar feature of the reduced center studied here must be stressed, that is, the relatively large inequivalence of the tensors, within each pair, especially between tensors $\mathbf{A}_3$ and $\mathbf{A}_4$ of the ferrous pair, the last one being peculiarly anisotropic. This is in contrast to the results reported in previous studies by Mössbauer on proteins with reduced (1+) active sites ligated to four cysteins (*17, 18*), for which the spectra have been interpreted on the basis of two equivalent iron atoms in each pair. The discrepancy can be explained, in part, by the fact that the ENDOR resolution is here very good, while being poor in Mössbauer. Moreover, with this last method, it is necessary to reduce the already large number of parameters of the fitting procedure.

(2) Theoretical Models

In this section, we will confine our discussion to the ^{57}Fe isotropic hyperfine coupling constants, laying aside the anisotropic parts. We already neglected them in our previous experimental work on the $[4Fe–4S]^{3+}$ species (*7*) as well as in our more theory-oriented article (*9*). These last terms are quite difficult to analyze because of the nature of the hyperfine contributions involved. Since the iron nuclei are at the heart of the spin population distribution, in contrast to the protons and ^{13}C of the CH_2 groups that are at its borders, their hyperfine tensors are the sum of two contributions of similar magnitude: one due to the electron orbital momentum, difficult to evaluate properly, and a second due to the electron spin momentum. Moreover, one must add that this problem is much more critical for the $[4Fe–4S]^{1+}$ state than for the $[4Fe–4S]^{3+}$ state. In effect, the hyperfine interactions with the nuclei of the ferrous pair have expected contributions due to the electron orbit of much more importance than that for the ferric pair of $[4Fe–4S]^{3+}$. This is why it appeared to us especially interesting to dispose of precise measurements of ^{57}Fe hyperfine tensors, postponing the theoretical computation of the orbital terms to a future work combining both experimental data and quantum-chemical calculations.

Iron–sulfur clusters can be described as coupled "FeS_4" high-spin monomers bearing spin $\vec{S}_{Fe}$ ($S_{Fe} = 2$ for Fe^{2+} and $\frac{5}{2}$ for Fe^{3+}). Then spin coupling coefficients $\{K(Fe)\}$ which reflect the way in which the local monomer spin $\vec{S}_{Fe}$ projects itself onto the total tetramer spin $\vec{S} = \Sigma_{Fe}\vec{S}_{Fe}$, are defined (*17*) as

$$K(\mathrm{Fe}) = \frac{\langle \vec{S}_{\mathrm{Fe}} \cdot \vec{S} \rangle}{\langle \vec{S} \cdot \vec{S} \rangle} \qquad [2]$$

with $\Sigma_{Fe}K(Fe) = 1$. The average $\langle\rangle$ in Eq. [2] is performed for a given cluster spin state. Concerning experimental ^{57}Fe hyperfine coupling constants $\{A_{iso}^{exp}(Fe)\}$, we decomposed them in a previous theoretical work (*9*) in the manner

$$A_{\mathrm{iso}}^{\mathrm{exp}}(\mathrm{Fe}) = K(\mathrm{Fe}) \cdot a(\mathrm{Fe}) = K(\mathrm{Fe}) \cdot d(\mathrm{Fe}) \cdot \bar{a}(\mathrm{Fe}), \qquad [3]$$

where a(Fe) stands as an "intrinsic" (i.e., free from spin coupling effects) ^{57}Fe hyperfine coupling constant. This quantity is usually thought to be dependent on the iron oxydation state only, and thus transferable from one iron–sulfur system to another. Typical values lie around -20 MHz (*9*). However, since a fraction of the spin population is delocalized on the sulfur ligands, the a(Fe) values also depend on the monomer covalency factor d(Fe), that is, on the fraction (normalized to unity) of unpaired spin located on the iron site once iron–sulfur covalency effects have been taken into account. We found the following covalency factor values, derived from DFT calculations (*11*): $d(Fe^{3+}) = 0.73$ and $d(Fe^{2+}) = 0.81$. The quantity $\bar{a}$(Fe) thus appears as the ionic equivalent of a(Fe), when covalency effects have been removed from it, that is, when $d(\mathrm{Fe}) = 1$.

Incidently, a previous theoretical analysis of ^{57}Fe isotropic hyperfine couplings (*9*) introduced the "site value"

$$a_{\mathrm{test}} = \sum_{\mathrm{Fe}} A_{\mathrm{iso}}^{\mathrm{exp}}(\mathrm{Fe}) = \frac{\sum_{\mathrm{Fe}} K(\mathrm{Fe}) \cdot a(\mathrm{Fe})}{\sum_{\mathrm{Fe}} K(\mathrm{Fe})} \qquad [4]$$

as a quantity useful for probing and comparing ^{57}Fe hyperfine couplings within the family of the iron–sulfur clusters of variable nuclearity. In effect, a common a(Fe) value for all iron sites results in $a_{test} = a(Fe) \approx -20$ MHz (*9*), whereas the occurrence of significantly different, though nondirectly observable site values, translates itself into a a_{test} value departing from the previously given average value.

Starting back from Eq. [3], the ionic value $\bar{a}$(Fe) contains two main physical contributions

$$\bar{a}(\mathrm{Fe}) = \bar{a}_{\mathrm{pol}}(\mathrm{Fe}) + \bar{a}_{\mathrm{orb}}(\mathrm{Fe}), \qquad [5]$$

that is, an isotropic core-polarization term $\bar{a}_{pol}$(Fe) arising from the polarization of the 1*s* to 4*s* shells ($\bar{a}_{pol}(Fe^{3+}) \approx -34.6$ MHz, $\bar{a}_{pol}(Fe^{2+}) \approx -37.8$ MHz) (*19, 20*), and a tensorial orbital term $\bar{a}_{orb}$(Fe), of which only the trace is considered here, expressed to first order as

$$\bar{a}_{\mathrm{orb}}(\mathrm{Fe}) = P(\mathrm{Fe}) \cdot \mathrm{Tr}\{\Delta\bar{g}(\mathrm{Fe})\}, \qquad [6]$$

where P is defined for an iron atom as the dipolar coupling constant between the ^{57}Fe nucleus and one of its 3*d* electrons: $P(Fe^{2+}) = 87.6$ MHz and $P(Fe^{3+}) = 98.7$ MHz (*9*) while $\Delta g(\mathrm{Fe}) = d(\mathrm{Fe})\Delta\bar{g}(\mathrm{Fe})$ stands as the local Fe **g** tensor corrected for the free electron value g_e (i.e., $\Delta g = g - g_e\mathrm{Id}$, where Id is the identity tensor).

(3) Summary of Proton Results

In order to perform the subsequent ^{57}Fe tensor analysis, it is appropriate to summarize here a few results obtained from the proton and ^{13}C ENDOR studies on the same redox species and compound (*11*). These studies have shown that there are indeed four thiolate ligands surrounding the [4Fe–4S] complex.

Moreover, the proton work reveals that a rotation of about 30° of one of the ligands (attached to Fe_3) has occured around the S–C bond when compared to the original diamagnetic compound.

The set of spin coupling coefficients are as follows: $K(Fe_1) = 1.48$, $K(Fe_2) = 1.82$, $K(Fe_3) = -1.03$, and $K(Fe_4) = -1.27$, extracted from the multicentric point–dipole analysis of the proton anisotropic hyperfine tensors. As a consequence, Fe_1 is more "ferrous" and Fe_2 is more "ferric" in the relative proportion 62/38%.

(4) Quantitative Analysis

It is useful, at first, to consider our present experimental data by computing the value of the parameter a_{test}. We find −28.6 MHz, which compares very well with both standard 4Fe-ferredoxin (−30.4 MHz) and aconitase-like (−28/−32 MHz) values. Therefore, our reduced species most probably presents the same hyperfine site values as in other comparable redox systems. Differences among these various systems must be sought therefore elsewhere.

Let us then first examine the hyperfine couplings relative to the atoms Fe_1 and Fe_2 attributed to the mixed-valence pair. As specified above, within each pair, there is no clue to assign each tensor to a definite iron atom. In this first pair, two possibilities have been considered. In the first case, tensor $\mathbf{A}_1$ is attributed to Fe_1 and $\mathbf{A}_2$ to Fe_2. A linear extrapolation of the inequivalence within the mixed-valence pair, applied to d(Fe) and $\bar{a}_{pol}$(Fe), yields $d(Fe_1) \approx 0.78$, $d(Fe_2) \approx 0.76$ and $\bar{a}(Fe_1) \approx -36.6$ MHz, $\bar{a}(Fe_2) \approx -35.8$ MHz.

From Eq. [3], $a(Fe_1) \approx -27.6$ MHz and $a(Fe_2) \approx -17.6$ MHz, that is, $\bar{a}(Fe_1) \approx -35.3$ MHz and $\bar{a}(Fe_2) \approx -23.2$ MHz. Considering now the second possible assignment ($\mathbf{A}_1$attributed to Fe_2 and $\mathbf{A}_2$ to Fe_1), one rather obtains $a(Fe_1) \approx -21.7$ MHz and $a(Fe_2) \approx -22.4$ MHz, that is, $\bar{a}(Fe_1) \approx -27.8$ MHz and $\bar{a}(Fe_2) \approx -29.5$ MHz. Finally, from $\bar{a}_{orb}(Fe) = \bar{a}(Fe) - \bar{a}_{pol}(Fe)$, $\bar{a}_{orb}$(Fe) can be evaluated for both hypotheses. The first assignment leads to $\bar{a}_{orb}(Fe_1) \approx +1.3$ MHz and $\bar{a}_{orb}(Fe_2) \approx +12.6$ MHz, whereas the second one leads to $\bar{a}_{orb}(Fe_1) \approx +8.8$ MHz and $\bar{a}_{orb}(Fe_2) \approx +6.3$ MHz. It then appears clearly that the first one is contradictory, since $|\bar{a}_{orb}(Fe_1)| < |\bar{a}_{orb}(Fe_2)|$, whereas Fe_1 is more "ferrous" and Fe_2 more "ferric". The second one is, in contrast, satisfactory and compares well with what was deduced for 4Fe-ferredoxins' data (*9*). This leads to assigning tensor $\mathbf{A}_1$ to Fe_2 and tensor $\mathbf{A}_2$ to Fe_1. Moreover, the main difference between Fe_1 and Fe_2 is one of spin-coupling coefficients, as the site $\bar{a}_{orb}$(Fe) values turn out to be very similar. The partial localization of the extra electron within the mixed-valence pair is therefore most probably due to some site energy difference between the two monomers (*21*). The thiolate ligand attached to Fe_1 is, in that respect, distinguished very significantly from the other three by its Fe–S–C–H dihedral angles (*13*).

Turning now our attention to the tensors $\mathbf{A}_3$ and $\mathbf{A}_4$ attributed to the ferrous pair, the same type of calculations can be developped. Identifying $\mathbf{A}_3$ and $\mathbf{A}_4$ with Fe_3 and Fe_4, respectively, one obtains $a(Fe_3) \approx -24.1$ MHz and $a(Fe_4) \approx -13.4$ MHz, whereas a typical standard 4Fe-ferredoxin value would be −18 MHz (*9*). The corresponding ionic quantities are given by $\bar{a}(Fe_3) \approx -29.7$ MHz and $\bar{a}(Fe_4) \approx -16.5$ MHz. Finally, from $\bar{a}_{orb}(Fe) = \bar{a}(Fe) - \bar{a}_{pol}(Fe)$, one computes $\bar{a}_{orb}(Fe_3) \approx +8.1$ MHz and $\bar{a}_{orb}(Fe_4) \approx +21.3$ MHz, whereas a typical standard 4Fe-ferredoxin value would be +13 MHz. With that identification, the orbital contribution of Fe_4 would be therefore quite unusual.

Identifying now $\mathbf{A}_3$ and $\mathbf{A}_4$ with Fe_4 and Fe_3, respectively, one rather obtains $a(Fe_3) \approx -16.5$ MHz and $a(Fe_4) \approx -19.5$ MHz. The corresponding ionic quantities are then given by $\bar{a}(Fe_3) \approx -20.4$ MHz and $\bar{a}(Fe_4) \approx -24.1$ MHz. Finally, from $\bar{a}_{orb}(Fe) = \bar{a}(Fe) - \bar{a}_{pol}(Fe)$, one computes $\bar{a}_{orb}(Fe_3) \approx +17.4$ MHz and $\bar{a}_{orb}(Fe_4) \approx +13.7$ MHz. In that case, the orbital contribution of Fe_3 would be slightly larger than expected, though not far from a typical value.

The second assignment, that is, $\mathbf{A}_4$ identified with Fe_4, seems to us more likely. In effect, all the intrinsic hyperfine values thus do not depart much from what is currently known. Moreover, as already stated in the previous section, the proton work revealed a unambiguous modification of the local ligand attached to Fe_3 with respect to the original diamagnetic compound. Finally, one can expect a substantial anisotropic orbital contribution as well for the iron atom corresponding to the $\mathbf{A}_4$ hyperfine tensor. Indeed, comparing both the $\mathbf{A}_3$ and $\mathbf{A}_4$ anisotropic tensors, it is clear that the magnitude of the latter one surpasses that of the former one (14.1 Vs 7.1 MHz for the largest of the three anisotropic values, for example). Assuming, as seems most reasonable, roughly same orders of magnitudes for the dipolar terms, the difference could be mainly ascribed to this orbital contribution.

V. CONCLUSIONS

In our previous work on Fe–S clusters where we attempted to develop a systematic analysis of ^{57}Fe hyperfine couplings for extracting semi-empirical spin projection coefficients, we noted the existence of two classes within the data pertaining to reduced "ferredoxin-like" [4Fe–4S] clusters (*9*). The first was labeled as "standard" (or "classical") ferredoxin data, with typical average hyperfine couplings of −30 MHz within the mixed-valence pair, and +15 MHz within the ferrous pair. The corresponding deduced spin coupling coefficients are +1.35 and −0.85, respectively. In the second class, that of "aconitase-like" systems, both hyperfine couplings and spin projection coefficients are of significantly larger magnitudes. As an example, for the aconitase-bound system, the following ^{57}Fe hyperfine coupling constants have been measured: $A(Fe_{b2}) \approx -36$ MHz, $A(Fe_{b3}) \approx -40$ MHz, $A(Fe_a) \approx +29$ MHz, and $A(Fe_{b1}) \approx +15$ MHz. A relatively large inequivalence of the iron parameters, especially within the ferrous pair, is observed for "aconitase-like" clusters.

The ^{57}Fe hyperfine values measured for the center I_R $[4Fe–4S]^{1+}$ cluster closely match the aconitase experimental ones. In contrast to the case of the aconitase-bound system, the four ligands are here chemically identical, being thiolates. In principle, one cannot exclude the fact that one of the ligands has been chemically modified, thus inducing anisotropy in the corresponding ^{57}Fe hyperfine coupling tensor. No additional ENDOR lines, pointing to the presence of some solvent molecule in the near vicinity of the paramagnetic cluster, has ever been detected. The only effect left is the distortion of the thiolate ligands by nearby crystalline deffects.

Even in that case, our proton work limits such distortions to a rotation of about 30° of ligand 3 (attached to Fe_3) around the S–C bond. This means two things for future [4Fe–4S] protein studies. First, one cannot directly deduce from the observation of inequivalence (within pairs) of iron hyperfine parameters that they have ligands of different nature. Second, these results illustrate quite well that deriving, just by proportionality, spin populations from the isotropic ^{57}Fe hyperfine couplings can lead to incorrect results. It is necessary to follow a cautious analysis of the ^{57}Fe hyperfine tensors along the lines presented above (*9*). As demonstrated here, this originates from the fact that one of the two ferrous hyperfine tensors (i.e., $\mathbf{A}_4$) presents a definitely large orbital contribution, and thus becomes atypical. As argued in Section IV-(4), we tentatively chose to assign $\mathbf{A}_4$ to Fe_3, on the basis of the fact that $\mathbf{A}_4$ presents an atypical orbital contribution most probably linked with this perturbation at the level of monomer 3.

Finally, as a side issue, and due to the difficulties of detecting here the transitions 4 under the best conditions possible (sharp lines, Q-band, etc.), we wish to emphasize the following point. Had this species been studied in a frozen solution and not in a single crystal, *one could very probably have missed these transitions and be led at best to difficulties in interpreting the ENDOR spectra, and at worst to attributing falsely the species studied here to a three-Fe cluster!* This may typically happen in ENDOR spectra of proteins and appears to us reminiscent of the Mo–Fe nitrogenase studies where ENDOR spectra corresponding to five ^{57}Fe were detected (*22, 23*), whereas earlier Mössbauer experiments (*24, 25*) suggested six iron atoms for the Mo–Fe prosthetic group. Only later did crystallographic determinations demonstrate that the cluster is actually made up of six iron and one molybdenum atom (*26, 27*). Therefore, the lesson to remember is that in iron–sulfur proteins, it is not possible to rely completely on ENDOR to determine the number of iron atoms in a cluster, except if resolution and sensitivity are both very good. Moreover, the results obtained by this method must be, as much as possible, brought together with those of Mössbauer studies where every iron atom weights equally in these spectra.

APPENDIX: SUPPLEMENTARY MATERIAL

The fit curves drawn on Fig. 3 correspond to expressions of the type $(A\cos^2\theta + B\sin^2\theta + 2C\sin\theta\cos\theta)^{1/2}$. The optimized parameters are now given for Tensors 1 to 3, fitting respectively high- and low-field points, and for Tensor 4 (only high field).

For the *c->*b* plane:**

Tensor 1	high field	$A = 476.43$	$B = 357.13$	$C = -22.19$
	low field	$A = 337.69$	$B = 241.88$	$C = -16.77$
Tensor 2	high field	$A = 337.16$	$B = 235.21$	$C = -2.45$
	low field	$A = 223.12$	$B = 143.66$	$C = -1.09$
Tensor 3	high field	$A = 249.34$	$B = 114.60$	$C = 12.81$
	low field	$A = 150.61$	$B = 54.85$	$C = 10.74$
Tensor 4	high field	$A = 123.47$	$B = 215.25$	$C = 116.33$

For the *c->*a* plane:**

Tensor 1	high field	$A = 478.38$	$B = 595.11$	$C = -12.12$
	low field	$A = 338.68$	$B = 431.92$	$C = -11.75$
Tensor 2	high field	$A = 340.47$	$B = 352.25$	$C = -15.87$
	low field	$A = 225.01$	$B = 230.01$	$C = -13.92$
Tensor 3	high field	$A = 251.70$	$B = 248.24$	$C = 54.63$
	low field	$A = 155.77$	$B = 150.46$	$C = 42.71$
Tensor 4	high field	$A = 110.63$	$B = 61.36$	$C = -46.45$

For the *a*′->b′ plane (low-field EPR line):

Tensor 1	high field	$A = 595.78$	$B = 370.00$	$C = -43.41$
	low field	$A = 432.62$	$B = 249.93$	$C = -34.22$
Tensor 2	high field	$A = 350.66$	$B = 241.30$	$C = -6.83$
	low field	$A = 228.30$	$B = 147.03$	$C = -3.72$
Tensor 3	high field	$A = 253.13$	$B = 117.14$	$C = -22.80$
	low field	$A = 154.10$	$B = 56.97$	$C = -16.59$
Tensor 4	high field	$A = 56.84$	$B = 178.41$	$C = 9.88$

For the *a*′->b′ plane (high-field EPR line):

Tensor 1	high field	$A = 595.41$	$B = 347.30$	$C = 36.13$
	low field	$A = 432.79$	$B = 234.36$	$C = 28.10$
Tensor 2	high field	$A = 350.73$	$B = 236.04$	$C = 0.37$
	low field	$A = 228.63$	$B = 145.10$	$C = -1.29$
Tensor 3	high field	$A = 253.80$	$B = 116.28$	$C = 36.09$
	low field	$A = 154.56$	$B = 55.05$	$C = 26.93$
Tensor 4	high field	$A = 55.50$	$B = 247.45$	$C = 16.16$

Hence:

$$\mathbf{gA}_1 + \mathbf{A}_1\mathbf{g} = \begin{pmatrix} 172.1 & -5.75 & -3.23 \\ -5.75 & 143.3 & -1.91 \\ -3.23 & -1.91 & 159.6 \end{pmatrix}$$

$$\mathbf{gA}_2 + \mathbf{A}_2\mathbf{g} = \begin{pmatrix} 129.1 & 0.07 & -4.09 \\ 0.07 & 113.9 & 2.13 \\ -4.09 & 2.13 & 131.5 \end{pmatrix}$$

$$\mathbf{gA}_3 + \mathbf{A}_3\mathbf{g} = \begin{pmatrix} 103.4 & -6.45 & 11.60 \\ -6.45 & 74.7 & 5.85 \\ 11.60 & 5.85 & 111.3 \end{pmatrix}$$

ACKNOWLEDGMENTS

We thank Mr. Gerard Desfonds for his excellent technical competence and his precious help in various aspects of the technical realization of this work. We are grateful to Dr. Schmalbein from Bruker (Karlsruhe) for the gift of an old

version of the ER 5106 QT variable temperature EPR cavity that we could adapt for ENDOR on single crystals.

REFERENCES

1. M. K. Johnson, "Encyclopedia of Inorganic Chemistry" (R. B. King, Ed.), Vol. 4, pp. 1896–1915, Wiley, Chichester, (1994).
2. H. Beinert, R. H. Holm, and E. Münck, *Science* **277,** 653–659 (1997).
3. H. Beinert, *JBIC* **5,** 2–25 (2000).
4. J. Gloux, P. Gloux, B. Lamotte, and G. Rius, *Phys. Rev. Lett.* **54,** 599 (1985).
5. J. Gloux, P. Gloux, B. Lamotte, J.-M. Mouesca, and G. Rius, *J. Am. Chem. Soc.* **116,** 1953–1961 (1994).
6. L. LePape, B. Lamotte, J.-M. Mouesca, and G. Rius, *J. Am. Chem. Soc.* **119,** 9757–9770 (1997).
7. G. Rius and B. Lamotte, *J. Am. Chem. Soc.* **111,** 2464 (1989).
8. J.-M. Mouesca, G. Rius, and B. Lamotte, *J. Am. Chem. Soc.* **115,** 4714–4731 (1993).
9. J.-M. Mouesca, L. Noodleman, D. A. Case, and B. Lamotte, *Inorg. Chem.* **34,** 4347–4359 (1995).
10. L. LePape, B. Lamotte, J.-M. Mouesca, and G. Rius, *J. Am. Chem. Soc.* **119,** 9771–9781 (1997).
11. F. Moriaud, S. Gambarelli, B. Lamotte, and J.-M. Mouesca, *J. Phys. Chem. B* **105,** 9631–9642 (2001).
12. Let us also add that, in order to complete this program, we have achieved ^{13}C studies by ESEEM-FT of this $[4Fe–4S]^{3+}$ same state (and also of the $[4Fe–4S]^{1+}$ center studied here), which will be published in the near future.
13. B. A. Averill, T. Herskovitz, R. H. Holm, and J. A. Ibers, *J. Am. Chem. Soc.* **95,** 3523–3534 (1973).
14. G. Denninger, private communication.
15. A. Schweiger, F. Graf, G. Rist, and H. Gunthard, *Chem. Phys.* **17,** 155–185 (1976).
16. A. Schweiger, *Struct. Bonding* **51,** 13–24 (1982).
17. P. Middleton, D. P. E. Dickson, C. E. Johnson, and J. D. Rush, *Eur. J. Biochem.* **88,** 135 (1978).
18. M. Belinskii, *Chem. Phys.* **176,** 15–36 (1993).
19. A. J. Freeman and R. E. Watson, "Magnetism" (G. T. Rado and H. Suhl, Ed.), Vol. IIA, p. 167, Academic Press, New York (1965).
20. R. E. Watson and A. J. Freeman, "Hyperfine Interactions," Academic Press, New York (1967).
21. X.-Q. Ding, E. Bill, A. X. Trautwein, H. Winkler, A. Kostikas, V. Papaefthymiou, A. Simopoulos, P. Beardwood, and J. F. Gibson, *J. Chem. Phys.* **99,** 6421–6428, (1993).
22. A. E. True, M. J. Nelson, R. A. Venters, W. H. Orme-Johnson, and B. M. Hoffman, *J. Am. Chem. Soc.* **110,** 1935–1943 (1988).
23. A. E. True, P. McLean, M. J. Nelson, W. H. Orme-Johnson, and B. M. Hoffman, *J. Am. Chem. Soc.* **112,** 651–657 (1990).
24. B. H. Huynh, E. Münck, and W. H. Orme-Johnson, *Biochim. Biophys. Acta* **527,** 192–203 (1979).
25. B. H. Huynh, M. T. Hentzl, J. A. Christner, R. Zimmermann, W. H. Orme-Johnson, and E. Münck, *Biochim. Biophys. Acta* **623,** 124–138 (1980).
26. J. Kim and D. C. Rees, *Science* **257,** 1677 (1992).
27. M. K. Chan, J. Kim, and D. C. Rees, *Science* **260,** 792 (1993).